AIP Advances

Implementation of full-area-deposited electron-selective TiO_X layers into silicon solar cells

Cite as: AIP Advances **8**, 125023 (2018); https://doi.org/10.1063/1.5061924
Submitted: 24 September 2018 . Accepted: 29 November 2018 . Published Online: 26 December 2018

Valeriya Titova, and Jan Schmidt

Implementation of full-area-deposited electron-selective TiO_x layers into silicon solar cells

Valeriya Titova[1,2,a] and Jan Schmidt[1,2]
[1]*Institute for Solar Energy Research Hamelin (ISFH), Am Ohrberg 1, 31860 Emmerthal, Germany*
[2]*Leibniz Universität Hannover, Institute of Solid-State Physics, Appelstr. 2, 30167 Hannover, Germany*

(Received 24 September 2018; accepted 29 November 2018; published online 26 December 2018)

We examine two different silicon solar cell designs featuring full-area electron-selective contacts based on ultrathin (2–3 nm) titanium oxide (TiO_x) films deposited by atomic layer deposition. The first cell design applies a layer stack to the cell front, which is composed of an ultrathin intrinsic amorphous silicon (*i*-a-Si:H) layer for interface passivation, the TiO_x film and an indium tin oxide (ITO) layer to provide a good lateral conductance for electrons to the metal fingers. Whereas carrier lifetime measurements on test structures promise high implied open-circuit voltages V_{oc} up to 726 mV, the realized solar cells achieve disappointingly low V_{oc} values <400 mV. The *J-V* parameters of this cell type are negatively affected by a reverse diode occurring due to the contacting of the TiO_x by the high-work function ITO layer. In the second cell type, we implement a layer stack to the cell rear, which is composed of an ultrathin silicon oxide (SiO_y) layer, the TiO_x film and a full-area-deposited aluminum (Al) layer. Initial V_{oc} values of these cells are relatively low (<600 mV), but improve significantly after annealing at 350°C. The best cell featuring a SiO_y/TiO_x/Al rear contact achieves an open-circuit voltage of 661 mV and an efficiency of 20.3%. No reverse diode is observed, which is attributed to the lower work function of the Al compared to ITO in the first cell design. From internal quantum efficiency measurements, we extract a rear surface recombination velocity S_{rear} of (52±20) cm/s for our best cell, which is well compatible with efficiencies exceeding 23%. https://doi.org/10.1063/1.5061924

I. INTRODUCTION

Compared to the implementation of dopant-diffused n^+ and p^+ regions used in most of today's industrial solar cells, there are several alternative materials that offer improved passivation of the silicon surface together with low contact resistances for majority carriers. These carrier-selective layers largely suppress contact recombination and, at the same time, allow an effective transport of majority carriers to the metal contacts.[1] In recent years, the application of TiO_x as electron-selective contact material to crystalline silicon (c-Si) has attracted increasing attention.[2–5] In particular, on test samples, very low surface passivation recombination velocities in combination with low contact resistances have been reported by several groups, leading to a calculated efficiency potential exceeding 26%.[5] This makes the application of TiO_x as electron-selective contact material potentially interesting for the next generation of highest-efficiency silicon solar cells. In this study, we examine the implementation of atomic-layer-deposited TiO_x into silicon solar cells. Two cell concepts are examined: one concept collects the electrons by the TiO_x layer at the cell front, the other one at the cell rear. In order to provide a good lateral conductance for the electrons, indium tin oxide (ITO) is deposited on

[a]Corresponding author: e-mail v.titova@isfh.de, Phone: +49 5151 999 635, Fax: +49 5151 999 400

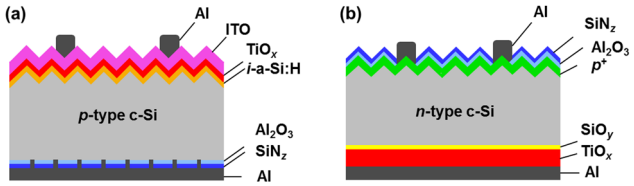

FIG. 1. Schematic of the two realized cell structures (a) on *p*-type silicon featuring a full-area electron-selective *i*-a-Si:H/TiO_x/ITO front contact and (b) on *n*-type silicon featuring a full-area electron-selective SiO_y/TiO_x/Al rear contact.

top of the TiO_x front layer and an ultrathin amorphous silicon (*i*-a-Si:H) layer is used between the c-Si surface and the TiO_x layer for improving the interface passivation. In the second cell concept, we deposit aluminum (Al) directly on top of the TiO_x rear layer and use an ultrathin silicon oxide (SiO_y) layer[5] between the c-Si surface and the TiO_x for improved interface passivation. We show that the use of a low-work-function material, such as Al, is essential for a good cell performance and the use of high-work-function ITO is leading to a reverse diode. Our results clearly prove that the SiO_y/TiO_x/Al full-area contact shows excellent properties concerning passivation and contact resistance and is hence well suited for the implementation to the rear of silicon solar cells.

II. SOLAR CELL FABRICATION

Figure 1(a) shows the first cell design examined in this study, where the TiO_x is implemented at the cell front. For this cell concept, we use single-side random-pyramid-textured (100)-orientated float zone (FZ) *p*-type silicon wafers with a resistivity of 1.3 Ωcm and a thickness of 300 μm. The rear side is processed using a standard PERC sequence.[6] First, the rear surface is coated by a 30 nm thick ALD aluminum oxide (Al_2O_3) layer deposited by plasma-assisted atomic layer deposition (PA-ALD) in a FlexAL system (Oxford Instruments) and subsequently a 100 nm thick silicon nitride (SiN_z) capping layer with a refractive index of 2.05 is deposited by plasma-enhanced chemical vapor deposition (PECVD) at 400°C in a Plasmalab80+ system (Oxford Instruments). Before the entire rear side is metallized by aluminum (Al), the Al_2O_3/SiN_z stack is locally opened by laser ablation. The opening geometry consists of points with a size of 420 × 420 μm^2 rectangularly arranged with a pitch of 1.5 mm and a total opened area of 4%. The front side is coated by a 2 nm thick intrinsic hydrogenated amorphous silicon (*i*-a-Si:H) layer deposited by PECVD (Cluster System CS 400 P, von Ardenne) and a 2 nm TiO_x layer. TiO_x is deposited using thermal ALD in a FlexAl reactor (Oxford Instruments) at a temperature of 230°C. Tetrakis(dimethylamino)titanium (TDMAT), H_2O and N_2 are used as titanium precursor, oxidant and purge gases, respectively. Subsequently, a 70 nm thick indium tin oxide (ITO) layer is sputtered on the front side followed by an aluminum grid evaporated through a shadow mask (1 mm finger spacing).

Figure 1(b) shows the second cell design examined in this work, where TiO_x is implemented at the cell rear. For this cell concept, 1.5 Ωcm *n*-type Czochralski (Cz)-grown silicon with a final thickness of 290 μm is used as base material. The front surface is random-pyramid-textured followed by boron diffusion with a sheet resistance of ~100 Ω/sq. Samples are stored in ambient environment for 3 months in order to grow a native silicon oxide (SiO_y) on the rear. In the next step, an Al grid is evaporated through a shadow mask on the cell front. Subsequently, 10 nm of Al_2O_3 (FlexAl reactor, Oxford Instruments) are deposited as a passivation layer and 52 nm SiN_z (Plasmalab 80+ reactor, Oxford Plasma Technologies) as an antireflection layer to the cell front. Afterwards, TiO_x is deposited on the rear using thermal ALD in a FlexAl reactor (Oxford Instruments) at a temperature of 230°C. Tetrakis(dimethylamino)titanium (TDMAT), H_2O and N_2 are used as titanium precursor, oxidant and purge gases, respectively. Finally, the entire rear surface is metallized on the full area with aluminum.

III. SOLAR CELL RESULTS

A. *i*-a-Si:H/TiO_x/ITO front cells

Figure 2 shows results of the cell design shown in Fig. 1(a) with *i*-a-Si/TiO_x front contact in combination with ITO (red circles). For comparison, the implied *J*-*V* curve (blue squares) measured

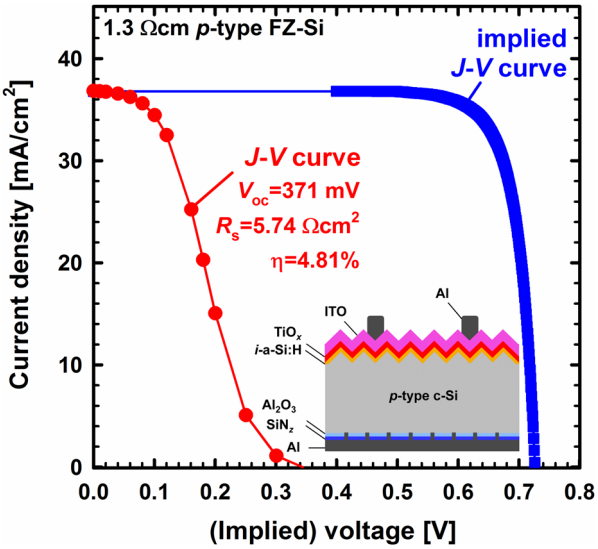

FIG. 2. Implied J-V curve deduced from symmetrical lifetime samples (blue squares) and measured one-sun J-V curve (red circles) of the best cell with i-a-Si:H/TiO_x/ITO front contact.

on symmetrical carrier lifetime samples with only i-a-Si/TiO_x but no ITO on both wafer surfaces is plotted as well. The implied J-V curve shows the V_{oc} potential of 726 mV measured on the lifetime sample. Disappointingly, on the realized solar cells we measure only a maximum V_{oc} of 371 mV. J-V measurements were performed at an illumination intensity of 100 mW/cm^2 at a temperature of 25°C using a commercial IV-tester (LOANA system, pv-tools, Hamelin, Germany). The implied J-V curves were deduced from carrier lifetime measurements performed using a Sinton WCT-120 tool (Sinton Instruments),[7] assuming the same one-sun short-circuit current density as measured on the best cell. The J-V curves of this cell type are negatively affected by a reverse diode occurring in the case of contacting by ITO, as was also observed on a similar cell structure by Boccard et al.[8] We assume that the high work function of ITO is not suitable for electron collection with TiO_x passivating contact layer.

B. SiO_y/TiO_x/Al rear cells

Table I summarizes the parameters of our best solar cells with a TiO_x thickness of 2 and 3 nm, respectively, measured after a post-annealing treatment at 350°C. All cells were measured using an aperture mask with an area of 2×2 cm^2. Our best cell with a 2 nm thick TiO_x shows a V_{oc} of 652 mV. The series resistance of 0.96 Ωcm^2 is resulting in a FF of 79.2%. Combining this value with a short-circuit current density of 38.7 mA/cm^2, an efficiency of 20.0% is achieved. The best solar cell of all fabricated devices in this study, which exhibits a V_{oc} of 661 mV, a J_{sc} of 38.7 mA/cm^2 and a FF of 79.2% resulting in an efficiency of 20.3%, is achieved with the 3 nm thick TiO_x layer, apparently due to its better passivation quality.

Figure 3 shows the measured one-sun J-V characteristic of our best solar cell (red circles). For comparison, the implied J-V curve (blue squares) as deduced from symmetrical lifetime test structures with SiO_y/TiO_x on both surfaces (but no Al metallization) is also included in Fig. 3. The implied J-V curve shows a V_{oc} potential of 694 mV. On the best realized solar cell, a V_{oc} of 661 mV is measured

TABLE I. One-sun cell parameters of the best solar cells with full-area TiO_x rear contact with an active area of 4 cm^2 measured after a post-annealing treatment at 350°C.

TiO_x thickness [nm]	V_{oc} [mV]	J_{sc} [mA/cm^2]	FF [%]	pFF [%]	η [%]	R_s [Ωcm^2]
2	652	38.7	79.2	82.2	20.0	0.96
3	661	38.7	79.2	82.6	20.3	1.11

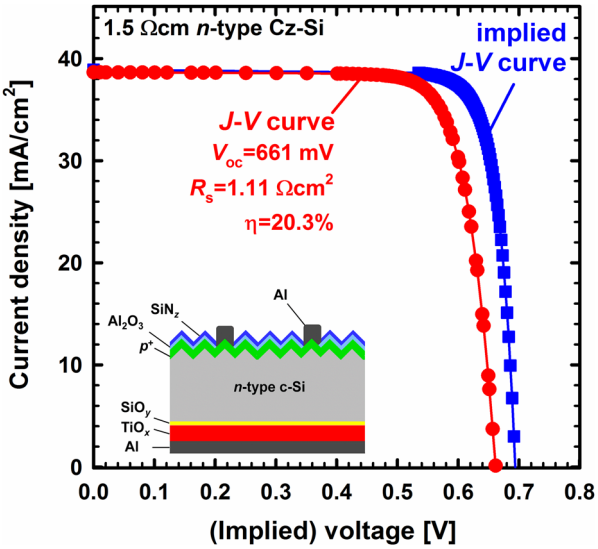

FIG. 3. Implied J-V curve deduced from symmetrical lifetime samples (blue squares) and J-V curve (red circles) of the best cell with the SiO_y/TiO_x/Al rear contact.

after the 350°C annealing step. The difference Δ between implied V_{oc} and realized V_{oc} is hence one order of magnitude lower (Δ = 33 mV) compared to the cell design incorporating ITO shown in Fig. 2 (Δ = 355 mV). The large difference in the Δ values obtained for the two different cell designs is most likely related to the fact that the ITO layer has a much higher work function (~0.3 eV) than the Al layer. Using a metal with a lower work function than Al could hence be a way to achieve even higher V_{oc} values and furhter reducing the Δ value, which is largely determined by the work function of the contact metal used.

Figure 4 clearly shows that the annealing treatment at 350°C for only one minute is an essential step for reducing the series resistance and thus improving the fill factor. The lowest

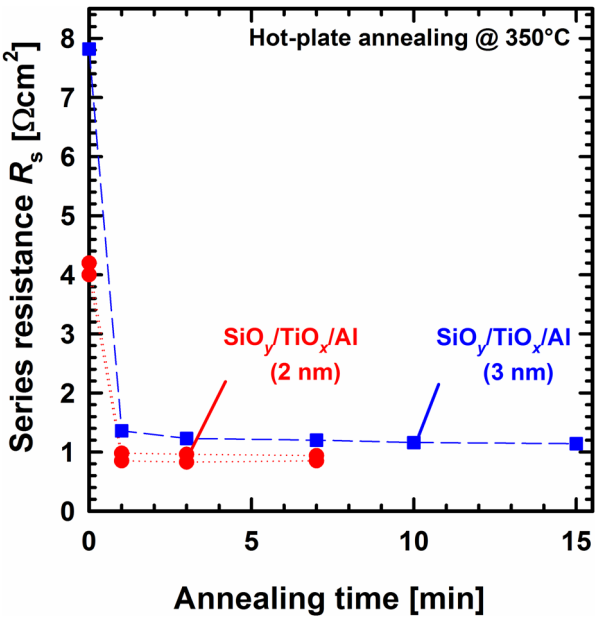

FIG. 4. Series resistance of the solar cells with SiO_y/TiO_x/Al electron-selective rear contact as a function of annealing time on a hot-plate at 350°C. In the cell batch solar cells with 2 nm TiO_x (red circles) and solar cells with 3 nm TiO_x (blue squares) were processed.

TABLE II. Measured one-sun cell parameters of the cell batch with two different metallization masks featuring a 'narrow' and a 'wide' busbar, respectively, after annealing on a hot-plate at 350°C. In this cell batch, solar cells with 2 and 3 nm TiO_x were processed.

Busbar	TiO_x thickness [nm]	V_{oc} [mV]	J_{sc} [mA/cm^2]	*FF* [%]	η [%]	R_s [Ωcm^2]
narrow	2	652	38.7	79.2	20.0	0.96
	3	661	38.7	79.2	20.3	1.11
wide	2	649	37.5	80.9	19.7	0.36
	3	651	38.3	80.9	20.2	0.50

series resistance value of 0.96 Ωcm^2 is achieved with a 2 nm thick TiO_x layer. For thicker TiO_x layers, the series resistance contribution increases to 1.1 Ωcm^2. Due to the higher V_{oc}, however, the efficiency of the cell with 3 nm TiO_x is slightly higher compared to the cell with 2 nm TiO_x.

To examine the efficiency potential of the SiO_y/TiO_x/Al stack as electron-selective contact system at the rear, solar cells with different metallization grids on the random-pyramid-textured front were fabricated. For this purpose, two different shadow masks with a finger distance of 1 mm and a finger width of 20 µm were used. The only difference of the two masks lies in the busbars: in the first case, the mask features a 'narrow' busbar which tapers from 20 µm at the top to 200 µm at the bottom, and in the second case the busbar features a 'wide' busbar which tapers from 200 µm at the top to 1000 µm at the bottom. The latter is intended to minimize the series resistance contribution of the front side in order to estimate the series resistance contribution of the the SiO_y/TiO_x/Al rear contact system.

Table II demonstrates that cells with a wide busbar show a slightly lower series resistance resulting in higher fill factor values. It is obvious that the major improvement in *FF* is achieved via low-temperature annealing at 350°C due a reduction in the series resistance.

Figure 5 shows the internal quantum efficiency (*IQE*) (closed symbols) and reflectance (open symbols) measured using the LOANA system of the best solar cell before (blue squares) and after annealing (red circles). In the wavelength range above 900 nm, the *IQE* of the solar cell measured in the as-deposited state is limited by a large rear surface recombination velocity of $S_{rear} > 6000$ cm/s. After the annealing step at 350°C, the *IQE* increases significantly and the extracted surface

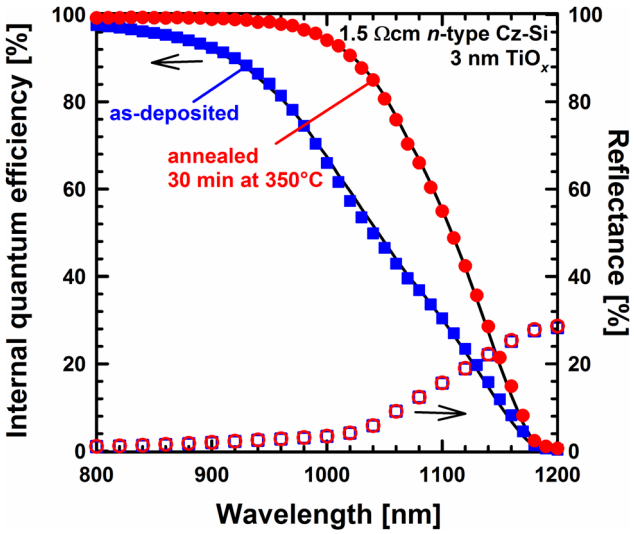

FIG. 5. Measured wavelength-dependent internal quantum efficiency (*IQE*) (closed symbols) and reflectance (open symbols) of the best *n*-type solar cell with 3 nm TiO_x on the rear in the as-deposited state (blue squares) and after annealing at 350°C (red circles). Black lines are fits to the measured data.

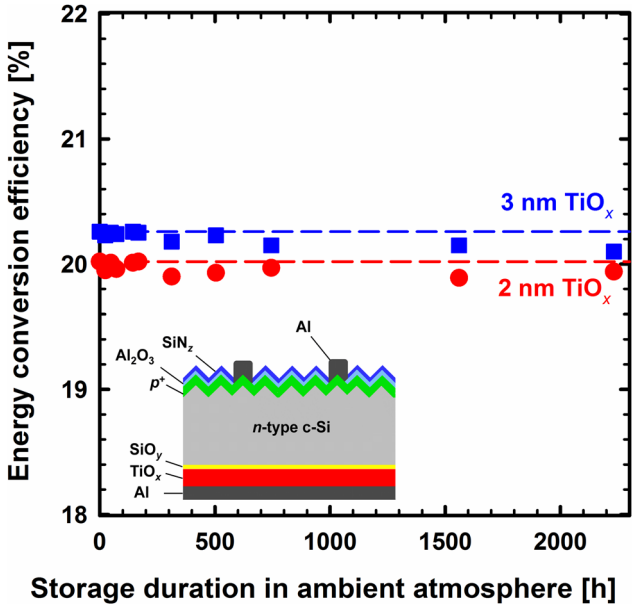

FIG. 6. Long-term stability of the best solar cells with 2 nm (red circles) and 3 nm (blue squares) TiO_x over time. In comparison, the measured efficiencies of the solar cells directly after annealing are also shown as dashed lines. The insert shows a schematic of the cell structure.

recombination velocity decreases to only S_{rear} = (52±20) cm/s. The S_{rear} values were extracted using the methodology of Brendel et al.[9] implemented into our in-house developed SCAN analysis software. The black lines shown in Fig. 5 are the corresponding fits to the measured *IQE* curves.

IV. LONG-TERM STABILITY

One major challenge of solar cells with heterojunctions made of alternative materials is their long-term stability in ambient atmosphere. We have hence examined the long-term stability of our best solar cells with the SiO_y/TiO_x/Al rear contact system.

Figure 6 shows the evolution of the efficiency of our best solar cells with a TiO_x thickness of 2 and 3 nm, respectively, after exposure to ambient atmosphere. As a reference, the efficiencies measured directly after annealing are shown as dashed lines. The direct comparison reveals that the efficiency after storage of the cells in ambient atmosphere over a long period of time (approx. 3 months) lies within the measurement uncertainty of ± 0.2%$_{abs}$ and the SiO_y/TiO_x/Al contact can hence be regarded as long-term stable.

V. CONCLUSION

In this study, two different silicon solar cell designs featuring full-area electron-selective contacts based on ALD-TiO_x were compared. The first cell design applied an *i*-a-Si:H/TiO_x/ITO layer stack to the cell front and in the second cell type, a SiO_y/TiO_x/Al stack was applied to the cell rear. The largely differing work functions of ITO and Al resulted in very low V_{oc} values for the ITO cell, but high V_{oc} values up to 661 mV for the cells with SiO_y/TiO_x/Al-contacted rear. The difference between implied V_{oc} and realized V_{oc} suggests that even higher V_{oc} values than 661 mV could be achieved by using a metal with an even lower work function than that of Al. From internal quantum efficiency measurements, we extract a rear surface recombination velocity of (52±20) cm/s for our best cell. Combining this very low rear surface recombination with a suitable low-work-function metal could hence result in efficiencies exceeding 23% for solar cells including TiO_x as electron-selective contact material.

ACKNOWLEDGMENTS

This work was supported by the German Federal Environmental Foundation (DBU) and the German State of Lower Saxony. We acknowledge the funding of this project within the PhD Scholarship Programme of the DBU. The authors thank Cornelia Marquardt for carrying out the boron diffusions. The publication of this article was funded by the Open Access Fund of the Leibniz Universität Hannover.

[1] J. Schmidt, R. Peibst, and R. Brendel, Solar Energy Materials and Solar Cells **187**, 39–54 (2018).
[2] J. Jhaveri, S. Avasthi, K. Nagamatsu, and J. C. Sturm, *Proceedings of the 40th IEEE Photovolt. Spec. Conf.* (Denver, 2014), pp. 1525-1528.
[3] X. Yang, K. Weber, Z. Hameiri, and S. De Wolf, Prog. Photovolt: Res. Appl. **25**, 896–904 (2017).
[4] T. Matsui, M. Bivour, P. Ndione, P. Hettich, and M. Hermle, Energy Procedia **124**, 628–634 (2017).
[5] V. Titova, B. Veith-Wolf, D. Startsev, and J. Schmidt, Energy Procedia **124**, 441–447 (2017).
[6] D. Zielke, J. H. Petermann, F. Werner, B. Veith, R. Brendel, and J. Schmidt, Phys. Status Solidi RRL **5**(8), 298–300 (2011).
[7] R. A. Sinton, A. Cuevas, and M. Stuckings, *Proceedings of the 25th IEEE Photovolt. Spec. Conf.* (Washington, 1996), pp. 457-460.
[8] M. Boccard, X. Yang, K. Weber, and Z. C. Holman, *Proceedings of the 43rd IEEE Photovolt. Spec. Conf.* (Portland, 2016), pp. 2403-2407.
[9] R. Brendel, M. Hirsch, R. Plieninger, and J. H. Werner, IEEE Transactions on Electron Devices **43**(7), 1104–1113 (1996).